A Conservation-Based Transitional Boundary Layer Model

M. Q. Brewster
Department of Mechanical Science and Engineering,
University of Illinois at Urbana-Champaign,
Urbana, IL 61801
e-mail: brewster@illinois.edu

A simple, flow-physics-based model of flat-plate, transitional boundary layer skin friction and heat transfer is presented. The model is based on the assumption of negligible time-, spanwise-, and streamwise-average wall-normal velocity at the top of the boundary layer. This results in a threefold increase in boundary layer thickness over the transition region. This simple velocity assumption and its boundary-layer growth implications seem to be reasonably consistent with more sophisticated (direct numerical simulation (DNS)) modeling simulations. Only two modeling parameters need to be assumed, the Reynolds numbers at the onset and at the completion of transition, for which there is guidance based on freestream turbulence intensity for smooth plates. Several experimental datasets for air are modeled. New criteria are proposed to help define the onset and completion of transition: zero net vertical (wall-normal) velocity or mass flux (integrated in time and space, spanwise and streamwise) at the top of the boundary layer, and tripling of boundary layer thickness. Also presented is a minor improvement to a previously published unheated starting length factor for flat-plate laminar boundary layers with uniform wall heat flux. [DOI: 10.1115/1.4054838]

Keywords: transitional boundary layer, laminar-turbulent transition, unheated starting length

1 Introduction

Simplified models of heat and momentum transport in wall-bounded, transitional boundary-layer flow usually involve fluid physics principles (conservation and transport rate considerations) from only the leading laminar and trailing fully turbulent regions but not the intermediate transition zone. This absence of transition-region physics is typified by idealized abrupt-transition textbook examples that violate physical conservation principles [1]. Extended transition models have generally relied on mathematical curve-fitting to patch together the mostly laminar and fully turbulent regions. An early example of an extended-transition curve-fit model is Churchill's 1976 paper [2], while a recent example is Lienhard's 2020 improvement [3] upon Churchill's model. The present paper offers a simplified model of extended transition-region wall heat transfer and shear stress with physical conservation—albeit rudimentary—as a basis. The germ for this idea was an unexpected finding and implication from Ref. [1] related to possible mass entrainment over the transition region via negative wall-normal velocity at the top of the boundary layer.

2 Uniform Wall Temperature (No Unheated Starting Length)

The modeling framework of the transitional boundary layer is shown schematically in Fig. 1. The boundary layer is mostly laminar up to x_L, which is the onset of transition. Instability and intermittency[1] begin at x_L and intensify as turbulence develops up to x_T after which point the boundary layer is assumed to be fully turbulent. Detailed structure of the transition flow is not considered. The type of transition is not distinguished. Freestream turbulence can modulate the process such that the transition can be ordered, bypass, or more complex. The wall is assumed to be aerodynamically smooth (no roughness effect) for turbulent flow modeling.

2.1 Laminar Region. The model used for the mostly laminar flow leading up to the onset of transition is the classical von Karman and Pohlhausen integral [4]. For streamwise velocity the following cubic profile is assumed over the laminar portion:

$$\frac{u}{u_e} = \frac{3}{2}\left(\frac{y}{\delta}\right) - \frac{1}{2}\left(\frac{y}{\delta}\right)^3, \quad x \le x_L \tag{1}$$

where u_e is the freestream velocity. This assumption introduces the (artificially finite or 100% as opposed to the typical 99%) boundary layer thickness δ. For this profile the displacement and momentum thicknesses relative to δ are $\delta_1/\delta = 3/8 = 0.375$ and $\delta_2/\delta = 39/280 = 0.139$, respectively. The mass conservation equation (integral in y, differential in x) is $\mathrm{d}\delta_1/\mathrm{d}x = v_e(x)/u_e$. The x-momentum equation (combined with mass conservation) is

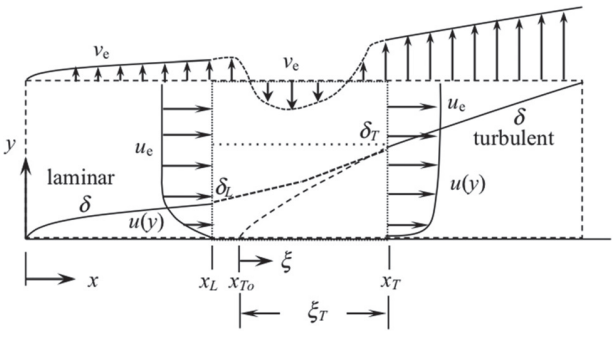

Fig. 1 Schematic diagram of transitional boundary layer model showing boundary layer thickness δ, virtual origin of fully turbulent boundary layer x_{To}, and velocity profiles, with time- and spanwise-average freestream wall-normal component v_e exaggerated compared with streamwise component u_e

[1]Intermittency is the time and spanwise average of a binary (0 or 1) indicator function based on the standard deviation of the sum of the magnitudes of the spanwise and wall-normal velocity components.

Contributed by the Heat Transfer Division of ASME for publication in the Journal of Heat Transfer. Manuscript received March 28, 2022; final manuscript received June 13, 2022; published online July 14, 2022. Assoc. Editor: Marc Hodes.

$d\delta_2/dx = C_f(x)/2$. Substituting Eq. (1) into the latter along with the Newtonian-fluid wall shear stress gives an ordinary differential equation (ODE) that can be solved for the boundary layer thickness

$$\frac{\delta(x)}{x} = \underbrace{\left(\frac{280}{13}\right)^{1/2}}_{4.64} \mathrm{Re}_x^{-1/2}; \quad \frac{\delta_L}{x_L} = 4.64\mathrm{Re}_{x_L}^{-1/2} \tag{2}$$

This result substituted in the definition of wall shear stress gives the skin friction coefficient

$$\frac{C_f}{2} = \underbrace{\frac{3}{2}\left(\frac{1}{4.64}\right)}_{0.323} \mathrm{Re}_x^{-1/2}; \quad \left.\frac{C_f}{2}\right|_{x_L} = 0.323\mathrm{Re}_{x_L}^{-1/2} \tag{3}$$

Similarly for heat transfer (assuming the ratio of thermal and hydrodynamic boundary layer thicknesses $r = \delta_t/\delta$ is of order one or smaller, which is reasonable for gases [4]) the corresponding temperature profile and results are

$$\frac{T - T_s}{T_e - T_s} = \frac{3}{2}\left(\frac{y}{\delta_t}\right) - \frac{1}{2}\left(\frac{y}{\delta_t}\right)^3, \quad x \le x_L \tag{4}$$

$$\frac{\delta_t(x)}{\delta(x)} = \frac{1}{1.026\mathrm{Pr}^{1/3}} \tag{5}$$

$$St_x = \underbrace{(1.026)(0.323)}_{0.332} \mathrm{Pr}^{-2/3}\mathrm{Re}_x^{-1/2}, \quad \mathrm{Re}_x \le \mathrm{Re}_{x_L} \tag{6}$$

and

$$\mathrm{St}_{x_L} = 0.332\mathrm{Pr}^{-2/3}\mathrm{Re}_{x_L}^{-1/2} \tag{7}$$

2.2 Fully Turbulent Region. The fully developed turbulent solution also comes from the classical integral solution but with an assumed 1/7-power streamwise velocity profile (time- and spanwise-average)

$$\frac{u}{u_e} = \left(\frac{y}{\delta}\right)^{1/7}, \quad x \ge x_T \tag{8}$$

For this profile the displacement and momentum thicknesses relative to δ are $\delta_1/\delta = 1/8 = 0.125$ and $\delta_2/\delta = 7/72 = 0.0972$, respectively. Because this profile is not valid near the wall and the y-derivative of u at the wall is unbounded, wall shear stress is evaluated using Prandtl's pipe flow expression for an aerodynamically (or hydraulically) smooth wall [4]

$$\frac{C_f}{2} = 0.0225\,\mathrm{Re}_\delta^{-1/4} \tag{9}$$

The turbulent boundary layer has a virtual origin at $x = x_{To}$ (which can be evaluated after the transition region is solved) such that it is convenient to use a shifted turbulent x-coordinate, ξ

$$\xi = x - x_{T_o} \tag{10}$$

in expressing the boundary layer thickness solution

$$\frac{\delta(\xi)}{\xi} = \underbrace{\left[\frac{5}{4}\frac{72}{7}(0.0225)\right]^{4/5}}_{0.371} \mathrm{Re}_\xi^{-1/5}; \quad \frac{\delta_T}{\xi_T} = 0.371\,\mathrm{Re}_{\xi_T}^{-1/5} \tag{11}$$

$$\frac{C_f}{2} = 0.0287\mathrm{Re}_\xi^{-1/5}; \quad \left.\frac{C_f}{2}\right|_{\xi_T, x_T} = 0.0287\mathrm{Re}_{\xi_T}^{-1/5} \tag{12}$$

Just as there is no surface roughness effect in Eq. (12), no freestream turbulence parameter ($\mathrm{Tu} = u'_{\mathrm{rms}}/u_e$) appears either (because none appears in Eq. (9)). Therefore, Eq. (12) should be presumed to apply only to relatively low-Tu freestream conditions and smooth wall conditions, with the possibility that it would break down at sufficiently high values of Tu and surface roughness.

For heat flux analysis, the 1/7-power mean-temperature profile

$$\frac{T - T_s}{T_e - T_s} = \left(\frac{y}{\delta_t}\right)^{1/7}, \quad x \ge x_T \tag{13}$$

has the problem, like the velocity profile, that it is not valid near the wall and the wall gradient is unbounded. This can be overcome by using an artificial combined laminar-plus-turbulent diffusivity (assumed to be the same for momentum and heat) that approaches zero at the surface and mathematically compensates for the artificial temperature gradient at the surface [4]. This artifice implicitly assumes that the turbulent momentum and thermal boundary layer thicknesses are equal; however, with an empirical correction for nonunity Pr

$$\frac{\delta_t(\xi)}{\delta(\xi)} = \frac{1}{\mathrm{Pr}^{2/5}} \tag{14}$$

the turbulent Stanton number [4] is

$$\mathrm{St}_\xi = 0.0287\mathrm{Pr}^{-2/5}\mathrm{Re}_\xi^{-1/5}, \quad \mathrm{Re}_x \ge \mathrm{Re}_{x_T}, \ (\mathrm{Re}_\xi \ge \mathrm{Re}_{\xi_T}) \tag{15}$$

$$\mathrm{St}_{\xi_T} = 0.0287\mathrm{Pr}^{-2/5}\mathrm{Re}_{\xi_T}^{-1/5} \tag{16}$$

2.3 Transition Region. The transition-region solution comes from control-volume integral balances (integral in both x and y) assuming the cubic laminar streamwise velocity profile at x_L and the 1/7-power streamwise turbulent velocity profile at x_T and assuming *zero net mass flow across the top, horizontal control surface*; that is, *negligible time-, spanwise- and streamwise-average vertical (wall-normal) velocity*. With this key assumption, the mass conservation equation gives the simple result that over the transition region the boundary layer thickness triples

$$\frac{\delta_T}{\delta_L} = 3 \tag{17}$$

and displacement thickness at the completion of transition is the same as at the onset, $\delta_{1_T} = \delta_{1_L} = (3/8)\delta_L$. From Eq. (17) the virtual origin of the turbulent boundary layer can be determined as

$$x_{T_o} = x_T - \xi_T, \ \mathrm{Re}_{\xi_T} = \underbrace{\left[\frac{3(4.64)}{0.371}\right]^{5/4}}_{92.9} \mathrm{Re}_{x_L}^{5/8} \tag{18}$$

With the aid of Eq. (18), the x-momentum balance over the transition region (still assuming *zero mass flow—and, therefore, zero x-momentum flow—across the top, horizontal control surface*) gives the increase in momentum thickness δ_2 and the average (over x_L to x_T) skin friction coefficient as

$$\frac{\delta_{2_T} - \delta_{2_L}}{x_T - x_L} = \frac{\overline{C}_f}{2} = \frac{16}{105}\left(\frac{\delta_L/x_L}{m-1}\right); \quad m = \frac{x_T}{x_L} \tag{19}$$

where δ_L/x_L is given by Eq. (2). The ratio m is a parameter indicating the relative extent of the transition zone. From experimental measurements of skin-friction coefficient and wall heat flux (see Sec. 4), the value of m, like the value of Re_{x_L}, depends on surface roughness, freestream turbulence, and freestream acoustic disturbance. Both Re_{x_L} and m are empirical parameters that must be assumed on a case-by-case basis. With the aid of Eq. (18),

Eq. (12) for the local wall shear stress and Eq. (16) for local heat flux at the end of the transition zone can be rewritten in terms of the assumed parameter Re_{x_L} as

$$\left.\frac{C_f}{2}\right|_{x_T} = 0.0116\mathrm{Re}_{x_L}^{-1/8}; \quad \mathrm{St}_{x_T} = 0.0116\mathrm{Pr}^{-2/5}\mathrm{Re}_{x_L}^{-1/8} \tag{20}$$

The average Stanton number over the transition region can either be derived from an integral (in both x and y) energy balance (still assuming *zero mass flow—and, therefore, zero energy flow—across the top, horizontal control surface*) or simply written by analogy as

$$\overline{\mathrm{St}} = \frac{16}{105}\mathrm{Pr}^{-1/2}\left(\frac{\delta_L/x_L}{m-1}\right) = \underbrace{\frac{16}{105}(4.64)}_{0.707}\frac{\mathrm{Pr}^{-1/2}}{(m-1)}\mathrm{Re}_{x_L}^{-1/2} \tag{21}$$

where the Pr exponent of –1/2 is an assumed intermediate value between the laminar value of –2/3 and the turbulent value of –2/5. Since the integral balances over the transition region do not yield local information, a reasonable way to approximate local behavior is to assume an $(x - x_L)^n$ power-law variation

$$\begin{aligned}\mathrm{St}_x - \mathrm{St}_{x_L} &= \frac{(\mathrm{St}_{x_T} - \mathrm{St}_{x_L})}{(x_T - x_L)^n}(x - x_L)^n \\ &= \frac{(\mathrm{St}_{x_T} - \mathrm{St}_{x_L})}{(\mathrm{Re}_{x_T} - \mathrm{Re}_{x_L})^n}(\mathrm{Re}_x - \mathrm{Re}_{x_L})^n,\ \mathrm{Re}_{x_L} \le \mathrm{Re}_x \le \mathrm{Re}_{x_T}\end{aligned} \tag{22}$$

with the value of the exponent n determined so as to match the average and end-point Stanton numbers over the transition zone

$$n+1 = \frac{(\mathrm{St}_{x_T} - \mathrm{St}_{x_L})}{(\overline{\mathrm{St}} - \mathrm{St}_{x_L})} = \frac{0.0116\mathrm{Pr}^{-2/5}\mathrm{Re}_{x_L}^{3/8} - 0.332\mathrm{Pr}^{-2/3}}{\frac{0.707}{(m-1)}\mathrm{Pr}^{-1/2} - 0.332\mathrm{Pr}^{-2/3}} \tag{23}$$

The complete solution for St_x is thus a combination of the laminar, transition, and turbulent solutions, Eqs. (6), (15), and (22).

3 Uniform Heat Flux (With Unheated Starting Length)

For the uniform heat-flux case, the right-hand sides of Eqs. (6) and (15) are increased by the factors 1.36 and 1.04, respectively [4], representing 36% and 4% increases in heat transfer coefficient relative to the uniform wall temperature case (the St_x coefficient changes are 0.332 → 0.453 and 0.0287 → 0.030 (or 0.0116 → 0.0121), respectively, for laminar and fully turbulent). The smaller effect of the wall boundary condition for the turbulent case goes along [4] with the weaker x-dependence of St_x, power of 1/5 versus 1/2, for turbulent compared with laminar. The question is, what to do for average Stanton number in the transition region, which has features of both flow types. A logical thing would be to expect that the effect of the wall boundary condition would be intermediate between that for laminar and fully turbulent flow; therefore, an increase of ~20% (midway between 36% and 4%) would seem reasonable, i.e., the right-hand side of Eq. (21) is multiplied by ~1.2 or coefficient change of 0.707 → 0.85. The other feature that needs addressing with the uniform wall-flux case is an unheated starting length, which was not included in the uniform wall-temperature case because none of the experimental data used below were reported as having this feature. However, the uniform wall heat flux experimental data do have this feature reported. With unheated starting length (x_0) included in the laminar portion (see Appendix A) the uniform wall flux solution is

$$\mathrm{St}_x = \frac{0.453\mathrm{Pr}^{-2/3}\mathrm{Re}_x^{-1/2}}{(1 - x_0/x)^{1/3}}, \quad \mathrm{Re}_x \le \mathrm{Re}_{x_L} \tag{24}$$

$$\mathrm{St}_{x_L} = \frac{0.453\mathrm{Pr}^{-2/3}\mathrm{Re}_{x_L}^{-1/2}}{(1 - \mathrm{Re}_{x_0}/\mathrm{Re}_{x_L})^{1/3}} \tag{25}$$

$$\mathrm{St}_\xi = 0.030\mathrm{Pr}^{-2/5}\mathrm{Re}_\xi^{-1/5},\ \mathrm{Re}_x \ge \mathrm{Re}_{x_T},\ (\mathrm{Re}_\xi \ge \mathrm{Re}_{\xi_T}) \tag{26}$$

$$\mathrm{St}_{x_T} = 0.0121\mathrm{Pr}^{-2/5}\mathrm{Re}_{x_L}^{-1/8} \tag{27}$$

$$\overline{\mathrm{St}} = 0.85\frac{\mathrm{Pr}^{-1/2}}{(m-1)}\mathrm{Re}_{x_L}^{-1/2},\ \mathrm{Re}_{x_L} \le \mathrm{Re}_x \le \mathrm{Re}_{x_T} \tag{28}$$

$$\mathrm{St}_x - \mathrm{St}_{x_L} = \frac{(\mathrm{St}_{x_T} - \mathrm{St}_{x_L})}{(\mathrm{Re}_{x_T} - \mathrm{Re}_{x_L})^n}(\mathrm{Re}_x - \mathrm{Re}_{x_L})^n,\ \mathrm{Re}_{x_L} \le \mathrm{Re}_x \le \mathrm{Re}_{x_T} \tag{29}$$

$$\begin{aligned}n+1 &= \frac{(\mathrm{St}_{x_T} - \mathrm{St}_{x_L})}{(\overline{\mathrm{St}} - \mathrm{St}_{x_L})} \\ &= \frac{0.0121\mathrm{Pr}^{-2/5}Re_{x_L}^{3/8} - 0.453\mathrm{Pr}^{-2/3}(1 - \mathrm{Re}_{x_0}/\mathrm{Re}_{x_L})^{-1/3}}{\frac{0.85}{(m-1)}\mathrm{Pr}^{-1/2} - 0.453\mathrm{Pr}^{-2/3}(1 - \mathrm{Re}_{x_0}/\mathrm{Re}_{x_L})^{-1/3}}\end{aligned} \tag{30}$$

4 Comparison With Experimental Measurements

Model calculations are compared with experimental measurements of local heat transfer coefficient in the form of Stanton number for air (Pr = 0.71) with both uniform wall temperature and uniform wall heat flux. Many datasets are available to choose from for air and for other fluids but not all studies report streamwise measurements of turbulence level. The three datasets chosen here [5–8] reported streamwise measurements of freestream turbulence intensity, $\mathrm{Tu} = u'_{\mathrm{rms}}/u_e$, which ranged, in the data used below, from 4% [7], when screens were used to induce turbulence, to 0.25% [8] without screens. Another parameter that could potentially influence transition in these data is surface roughness. Two of the studies [5,6,8] reported efforts to prepare smooth surfaces, varnished copper [6], and painted stainless steel foil [8]; the other [7] did not and probably used "as-received" brass, which could have induced roughness effects.

4.1 Uniform Wall Temperature. Figure 2 shows local Stanton number results for uniform wall temperature. Model calculations are compared with experimental data [5–7]. The experimental data are from two sources, Reynolds et al. [5,6] and Kestin et al. [7]. Shown with each dataset is the reported

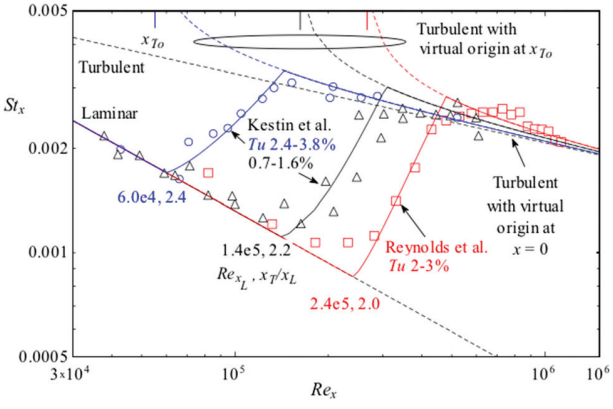

Fig. 2 Local Stanton number versus Reynolds number for uniform wall temperature; model calculations from Eqs. (6), (15), and (22) with assumed parameters Re_{x_L} and x_T/x_L compared with experimental data with varying turbulence intensity Tu from Reynolds et al. [6] and Kestin et al. [7].

freestream turbulence intensity level, Tu. Generally, the onset of transition occurs earlier (lower Re_{x_L}) for higher Tu.

In the Reynolds studies [5,6], independently heated copper strips [5] were used to seek uniformity of wall temperature. Most of the data were for early transition conditions in which emery cloth strips were used to trip turbulence [6]. In one dataset [6] the emery cloth was removed and "natural transition" was allowed to occur; this is the dataset appearing in Fig. 2. The copper surfaces were "varnished and rubbed down several times to give a hydraulically smooth surface [5]." Otherwise, no screens were used to induce freestream turbulence, which was reported as being between 2 and 3%, with higher values occurring at higher velocities and at the leading edge of the plate [5]. The freestream speed of the natural transition data can be inferred as 12 m/s (39 ft/s) from the mass flux data [6].

In the Kestin et al. [7] data, steam heating was used to seek uniformity of wall temperature. Two electrical heaters were used to measure heat flux at locations that divided the plate in thirds lengthwise (streamwise). A range of freestream speeds was used from 4 to 38 m/s. A screen was sometimes used to increase the turbulence level in the wind tunnel. Without the screen, the turbulence level ranged from 0.7 to 1.6%. With the screens in place turbulence intensity was 3.1–3.8% at the upstream heater location and 2.4–3.0% at the downstream heater location. The plate surface was brass. The surface condition (e.g., polishing) was not mentioned.

Figure 2 shows that within the two Kestin et al. datasets the location of the onset of transition is consistent with expectations based on the freestream turbulence intensity. The Reynolds et al. dataset, however, with Tu of 2–3%, exhibits transition at even higher Reynolds numbers than the low-Tu (0.7–1.6%) Kestin et al. dataset. Clearly other factors than just freestream turbulence influence the onset of transition. Perhaps differences in surface roughness played a role; e.g., perhaps a less-than-smooth surface in Kestin et al. influenced onset in their data.

The model calculations are shown by solid lines in Fig. 2, with the assumed Re_{x_L} and m ($= x_T/x_L$) values accompanying each of the three curves. The onset Reynolds number ranges from 60,000 to 240,000. The m value is approximately 2; that is, the transition zone is approximately as long as the leading laminar portion. However, m is not constant. As Re_{x_L} increases, m decreases, in Fig. 2 from 2.4 to 2.0. The values of the exponent n from Eq. (23) for the three cases in Fig. 2 from low to high onset Reynolds number are $n = 1.23$, 1.53, and 1.30. The model predicts slight "overshoot" in St_x at the beginning of the fully turbulent region (the term overshoot has been used to mean St_x above that for the turbulent solution assuming virtual origin at $x = 0$). Overshoot is also exhibited in two of the experimental data sets, Reynolds et al. and Kestin et al. high-Tu, but not with the sharpness exhibited by the simple model at this junction between the end of the transition zone and the beginning of the fully turbulent zone. A similar shortcoming of this simple model is also evident at the other junction, the beginning of the transition zone, where the experimental data trend is smoother and model predictions too sharp. This region is problematic, however, because experimental data do not always exhibit a smooth trend line. For example, there is a datum point in the high-Tu data of Kestin et al. at $Re_x = 66{,}300$ (an open circle in Fig. 2 lying on the laminar solution line with $St_x = 0.0016$, $Nu = 76.6$, in Ref. [7], Table 1) that could be interpreted as an outlier with respect to the trend of the next neighboring open-circle datum point which has slightly higher Re_x of 71,100 and noticeably higher St_x of 0.0021 ($Nu = 105.2$ [7]). Yet other than this appearance of data scatter there is no reason to discard either the higher or lower point (no information in the raw data would disqualify either; they just happened to be measured at different heaters; the lower point was measured at the upstream heater and the higher point at the downstream heater [7]). Yet if either of these two points were missing from the plot, the interpretation of the trend and model fit would be very different. Without the lower point, for example, a more gradual slope for St_x versus x would fit the experimental data better, which is what seems to be happening in Fig. 2 of Ref. [3], where the lower point (an open triangle in Fig. 2 of Ref. [3]) appears to be obscured by other data point symbols.

Aside from the two transition junction regions, that is, away from the beginning (onset) and ending (completion) of the transition region, in the middle of the laminar, transition, and turbulent regions, the model generally matches the experimental data well, even in spite of freestream turbulence up to Tu ~ 3 to 4% (Eqs. (9)–(11) are for negligible Tu effect.) An exception is the lowest point of the Reynolds et al. data ($Re_x = 82{,}000$). This point can possibly be considered an outlier since the raw data [6] show that the plate temperature was below average at that location. Or perhaps this point exhibits some amount of unheated starting-length effect, which is seen more prominently in the next data of Fig. 3.

4.2 Uniform Wall Heat Flux. Figure 3 shows local Stanton number results for uniform wall heat flux. Model calculations are compared with experimental data from Blair [8]. Blair used electrically heated stainless steel foil to generate uniform wall heat flux. The foil was painted flat black and reported to be aerodynamically smooth. The heating arrangement was such that there was an unheated starting length of 4.3 cm. The freestream speed was constant at 30.3 m/s such that Re_{x_0} in Eqs. (25) and (30) is 86,900. Apart from the unheated starting length, trends and comparisons for the uniform heat-flux case are mostly similar to those noted above for uniform wall temperature. The model calculations are shown by solid lines in Fig. 3, with the assumed Re_{x_L} and m ($= x_T/x_L$) values accompanying each of the three curves. The onset Reynolds number ranges from 200,000 to 1,600,000, increasing as turbulence intensity decreases. The m value is approximately 2, decreasing as the onset Reynolds number increases: $m = 2.2$, 2.0, and 1.67. The values of the exponent n from Eq. (30) for the three cases from low to high onset Reynolds number are $n = 3.12$, 2.05, and 1.23. Some overshoot in St_x is seen at the end of the transition zone, at least for the two higher turbulence cases, 1% and 2%, which, like all the cases in Fig. 2, are probably bypass transitions. In general, model calculations are too sharp at the beginning and ending junctions of the transition region but otherwise good in between. One exception is at the transition onset for the low (0.25%) turbulent case, which is probably an ordered (Tollmien–Schlichting wave) transition, where the rise in St_x is sudden and sharp and the model more closely matches the trend than in the bypass transition cases. Another unique feature of Fig. 3 is that the unheated starting length effect is clearly seen, which causes St_x to increase above what it would be without the unheated start to the boundary layer.

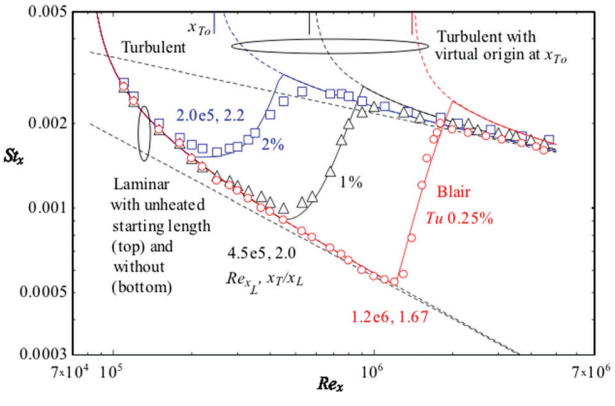

Fig. 3 Local Stanton number versus Reynolds number for uniform wall heat flux; model calculations from Eqs. (24), (26), and (29) with assumed parameters Re_{x_L} and x_T/x_L compared with experimental data with varying turbulence intensity Tu from Blair [8].

5 Discussion

In comparing the data between Figs. 2 and 3 for consistency of transition behavior, it appears that the Reynolds et al. data and the Blair data are consistent with each other; the Reynolds data (Tu = 2–3%) and the highest-Tu Blair data (Tu = 2%) have comparable transition Reynolds-number parameters, and the lower-Tu Blair data exhibit more delayed onset as expected. The Kestin et al. data do not seem consistent with the Reynolds et al. and Blair data in terms of transition parameters (as noted above relative to just the Reynolds et al. data). It could be that the Reynolds et al. data and Blair data exhibit transition behavior for truly smooth surfaces, where only freestream turbulence influences transition; whereas the Kestin et al. data exhibit influences of both freestream turbulence and surface roughness. Recall that the surface in Kestin et al. was only reported as being brass without mentioning surface condition. A similar apparent inconsistency can be found in comparing the Kestin et al. data with data from another study, Junkhan and Serovy [12], as in Ref. [3]. Figure 2 of Ref. [3] compares the low- and high-Tu datasets from Kestin et al. with low- and high-Tu sets, from Junkhan and Serovy, Fig. 4 from Ref. [12]. The Tu levels reported in each study are (from low to high Tu): Junkhan low-Tu: 0.4 to 0.8%; Kestin low-Tu: 0.75 to 1.6%; Junkhan high-Tu: 1.3–1.8%; Kestin high-Tu: 2.4–3.8%. If only Tu mattered the ordering of the onset of transition should follow the order of the reported Tu levels just listed (which included the effect of axial decay of Tu). From Fig. 2 of Ref. [3], it can be seen that the ordering of transition onset between the two low-Tu sets is consistent with the assumption that only freestream turbulence affects onset. However, the ordering between the two high-Tu sets does not. The Junkhan and Serovy high-Tu set (Tu = 1.3–1.8%) should show onset earlier (at lower Reynolds number) than the high-Tu Kestin et al. set (Tu = 2.4 to 3.8%), not later. This is another indication that something other than freestream turbulence—perhaps surface roughness—is playing a role in the onset of these experimental data. In Junkhan and Serovy, the plate was Nichrome alloy but nothing was reported about roughness or surface preparation so apparently, the surface was as received. As-received surfaces, Nichrome, in the case of Junkhan et al., or brass, in the case of Kestin et al., may seem aerodynamically smooth (behavior independent of roughness) but they may not behave that way for transition-onset purposes. If roughness effects are present in the onset behavior of the data of Kestin at al., those effects are not apparent in the fully turbulent skin friction behavior, just like there are no apparent effects of freestream turbulence on fully turbulent skin friction, at least at these levels of Tu (< 4%). Thus, there remain open questions in comparisons between model calculations that assume smooth wall (no roughness effect) in the turbulent zones of a transitional boundary layer compared with experimental data for which surface roughness is not sufficiently documented.

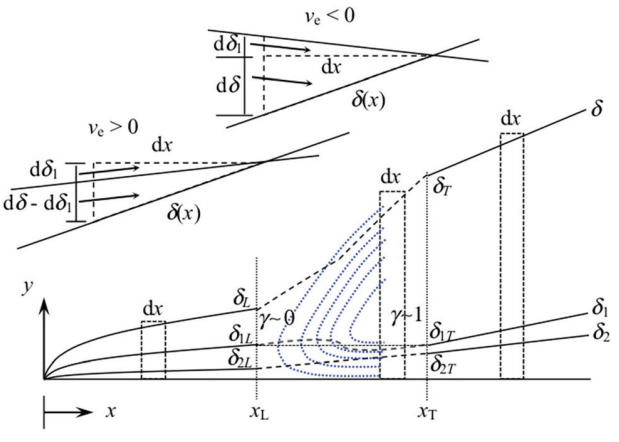

Fig. 4 Schematic diagram of transitional boundary layer model showing boundary layer thickness δ, displacement thickness δ_1, momentum thickness δ_2, and intermittency contours γ. Insets show time- and spanwise-average flow at top of boundary layer for transition core ($v_e < 0$) and elsewhere ($v_e > 0$).

The feature of overshoot in St_x at the end of the transition region was noted above and has been observed and discussed elsewhere [9,10]. Overshoot is clearly a real phenomenon as indicated by both experimental observations [6–9] and direct numerical simulations (DNS) [9], in both heat flux [9] and skin friction [10]. The simple explanation usually offered is that overshoot is a result of the virtual origin of the fully turbulent boundary layer occurring at an x-location somewhere downstream of the leading edge. While this statement is true, it lacks specificity of physical explanation. More mechanistic descriptions include that overshoot [9] "results from evolution of large-scale laminar disturbances to finer scale turbulence, during which locally enhanced shearing and heat transfer occur." The fact that the present simple model does not match overshoot in experimental data well is built into the model by the artificially abrupt junction at the end of the transition region. No numerical smoothing at the junction is built into the model, as was done in Refs. [2] and [3]. Neither is any smoothing transport mechanism built into the model, such as streamwise turbulent diffusion, which is likely responsible physically for smoothing velocity and temperature gradients axially.

At the beginning junction of the transition region, the mismatch in modeling and experimental results for St_x was also noted above. Indeed, deviation from purely laminar or Blasius flow is expected and can be attributed to various phenomena including Tollmien–Schlichting waves (Tu < 0.5%) and Klebanoff streaks (Tu > 0.5%) [10]. If matching these types of flow features with a simple model were the objective (which it is not here) then numerical curve-fitting or more refined physical modeling could be employed. Indeed, there are many complex phenomena entailed in transitional flow that such a simple model as this is not meant to address. For example, incipient turbulent flow within turbulent spots can occur away from the wall before growing and its statistics differ substantially from the fully developed turbulent flow. The laminar flow surrounding the spots can experience additional stresses due to entrainment in the relaxation region of turbulent spots and under the so-called overhang region at the front of a spot and thus quantities such as the skin friction are elevated notably. These flow features probably account for at least some of the mismatch in modeling and experimental results.

The unique feature of the present model is the physical assumption about negligible time-, spanwise-, and streamwise-average wall-normal (vertical) velocity at the top of the transitional boundary layer and the associated threefold growth in boundary-layer thickness. Further consideration of this key assumption is warranted. Consider a rectangular differential-integral control volume from x to $x + dx$ and from $y = 0$ to $\delta + d\ \delta$ as shown in Fig. 4. Consider further the small triangular portion at the top, which is bounded on the bottom by the boundary layer thickness $\delta(x)$, with slope $d\delta/dx$, on the left by a vertical surface of height $d\delta$, and on the top by a horizontal surface of length dx. Through this triangle, for laminar and fully turbulent flows (see inset diagram: $v_e > 0$), run streamlines (time- and spanwise-average flow) that are nearly horizontal but which have a slightly upward slope in the streamwise direction because of a small, positive vertical component of velocity. Consider one such streamline that passes through the upper right point $(x + dx,\ \delta + d\ \delta)$. By the integral-differential mass conservation equation and definition of displacement thickness $\delta_1(x)$, this streamline has slope $d\delta_1/dx$ (as do all streamlines); therefore it intersects the left surface at a point that divides that surface into upper and lower segments of lengths $d\delta_1$ and $d\delta - d\delta_1$, respectively. The ratio $d\delta_1/d\delta$ represents the fraction of the flow entering the left face that passes out the top of the triangle. Similarly, $1 - d\delta_1/d\ \delta$ represents the fraction of the flow entering the left face that crosses $\delta(x)$ into the boundary layer. For flat-plate laminar and turbulent boundary layers the fractions $d\delta_1/d\delta$, by this analysis, are 0.375 and 0.125, respectively. Over the laminar-

turbulent transition region, the flow undergoes adjustment from conditions where the higher fraction, 0.375, prevails to those where the lower fraction, 0.125, does. The question is, over the transition region, as this adjustment is happening, on average (time, spanwise, and streamwise), what is the fractional flow split? The answer depends on the magnitude and sign of v_e. As the flow enters the transition region it is likely that v_e remains positive but not for very long. As depicted in Fig. 1, in the core of the transition there is a region where time- and spanwise-average v_e is negative (see Fig. 4 inset diagram: $v_e < 0$) before it turns positive again and transitions into the fully turbulent behavior. The postulate made here is that for practical purposes (simplified modeling calculations) it is sufficiently accurate to assume that the net vertical mass flow across the horizontal control surface is zero. Essentially all the inflow passes into the boundary layer, with negligible amount passing out the top, causing the boundary layer to grow at a rate faster than that even for a fully developed turbulent boundary layer.

To quantify the rapid rate of increase of boundary layer thickness in the transition zone relative to that in a fully developed turbulent boundary-layer consider over what length does a turbulent boundary layer triple in thickness and how does this compare with the transition region length? Working nondimensionally in Reynolds number, for Re_{x_L} of 3×10^5, Eq. (18) gives Re_{ξ_T} of approximately the same magnitude, 2.46×10^5, and with some algebra, it can be shown that the Re_ξ value where the turbulent boundary layer has grown three times in thickness from the value at ξ_T is approximately 70 times Re_{ξ_T}, which is significantly more than the transition length of about one or at most two times Re_{ξ_T}. Thus the rate of boundary-layer growth is significantly faster in the transition region than anywhere else in the boundary layer.

Though it is not part of the model it is instructional to consider the streamwise variation of displacement thickness, $\delta_1(x)$. Given the x-variation of $v_e(x)$ that is sketched in Fig. 1, the x-variation of $\delta_1(x)$, as determined by the integral-differential mass balance, $\mathrm{d}\delta_1/\mathrm{d}x = v_e(x)/u_e$, is shown in Fig. 4, a curve slightly deviated from a horizontal line between the endpoint value $\delta_{1_T} = \delta_{1_L}$, with a leading portion slightly above the horizontal line and a trailing portion slightly below. In the core region of the transition, where v_e is negative, so is $\mathrm{d}\delta_1/\mathrm{d}x$, which is opposite usual boundary layer behavior. This is the region that provides most of the mass inflow that enables the laminar profile in streamwise velocity $u(y)$ to transition to the fuller turbulent one.

DNS studies of transitional boundary layer behavior give evidence that supports the present modeling approach. DNS results of the rate of boundary-layer growth [11] and of ensemble-average velocities in the boundary layer [10] corroborate the present model's key assumption. Figure 3 of Ref. [11] shows contours of the intermittency field γ, which ranges from 0 (no intermittency or laminar flow) to 1 (complete intermittency or turbulent flow) in a transitional boundary layer. To give a better idea, similar intermittency isosurfaces are sketched in Fig. 4. Figure 3 of Ref. [11] also includes a dashed line representing the growing boundary layer thickness, which shows a threefold increase in boundary-layer thickness, going from nondimensional values of 10∼12 to 30∼36, over the transition region, with a noticeable change (increase) in the slope of $\delta(x)$ at x-values where the x-component of gradient in γ is steepest. As for wall-normal velocities, Fig. 27 of Ref. [10] shows contours of ensemble-average velocity components in a transitional boundary layer, including streamwise, spanwise, and wall-normal (vertical) components in and near a turbulent spot. The authors' observations [10] about the velocity field have particular relevance to the present modeling approach: "The streamwise component captures the fuller [turbulent] velocity profile in the center of the spot, and how it gives way to laminar velocities in the rear and front parts. The vertical velocity shows an interesting trend: it is positive only in a limited region near the spot center, where the boundary layer is closest to a fully turbulent state; toward the rear and front parts of the spot, the vertical velocity is negative, which is required in order to transition the streamwise velocity profiles from the laminar to a fuller turbulent shape." This is important because significant regions of negative wall-normal velocity would be necessary in the transitional boundary layer for there to be negligible streamwise-average wall-normal velocity (negligible mass flow) at the top of the transitional boundary layer.

The basic idea for the present simple model came from an unexpected finding in Ref. [1] related to the intriguing idea of possible mass entrainment over the transition region via a negative wall-normal velocity component at the top of the boundary layer. At first, this assumption may seem incorrect and may require some getting used to because classical boundary-layer theory, even turbulent time-averaged, so engrains the idea of positive vertical velocity and mass flow out the horizontal top of a control volume. In retrospect, the present model is actually an extended-transition version of case-02 of Ref. [1], in which continuous displacement thickness was assumed across a collapsed (abrupt) transition, corresponding to zero mass flux at the top, and a discontinuous momentum thickness (and enthalpy thickness) was assumed with a jump corresponding to transitional wall shear stress (and wall heat flux). For the present extended-transition model, the evolution of displacement and momentum thicknesses are shown schematically in Fig. 4. As noted above, displacement thickness likely increases initially, then decreases, then increases again such that at the end it is the same as at the onset at $\delta_{1_T} = \delta_{1_L} = (3/8)\delta_L$. Momentum thickness experiences a monotonic increase, the overall value of which, from Eq. (19), and in ratio form, is independent of x_L and x_T as $\delta_{2_T}/\delta_{2_L} = 1 + 128/117 = 2.09$.

Because of its simplicity, the assumption of no vertical mass flow at the top of the boundary layer over the transitional region may seem to introduce modeling inaccuracy, as when modeling approximations are introduced in general. But this is only if we think of onset and completion of transition as independently well-defined conditions, which they are not. There is latitude in defining x_L and x_T and therefore, as long as we accept that the time- and spanwise-average wall-normal velocity v_e varies as indicated in Fig. 1, going both above and below zero, the mean value theorem guarantees there to be a range of x_L and x_T values that would give a streamwise-average v_e value of zero over x_L to x_T. *It would seem that there exist reasonable transition onset and completion x-values ($x_{L,T}$) over which the vertical net mass flow is zero and over which the transitional boundary layer thickness approximately triples*. These conditions could even be among the criteria used to define the onset and completion of transition; the traditional 99% boundary layer thickness should be satisfactory for this purpose.

Finally, the purpose of this paper is to present the main concept of this simple model, which is negligible time-, spanwise-, and streamwise-average wall-normal velocity at the top of a wall-bounded, transitional boundary layer. The purpose is not to attempt to use this simple model to explain complicated transitional turbulent flow features. In discussing the comparisons between this simple model and experimental results, the possible influences of two factors that are not in the model, surface roughness and freestream turbulence, were brought up. That discussion was meant to be speculative, not definitive, as there is no experimental evidence to back it up. Furthermore, there are likely other factors besides these two that could play a role but that has not been mentioned here. This model is proposed as a rudimentary tool to describe transitional flows for which surface roughness effects are negligible and freestream turbulence intensity is minimal using just two parameters, the Reynolds numbers at the onset and completion of the transition region.

6 Summary

In summary, the capability of a simple new, flow-physics-based model of flat-plate, transitional boundary-layer skin friction and heat transfer has been demonstrated by matching several experimental datasets. The model is textbook simple; it respects

conservation principles and embodies transitional boundary-layer physics that are reasonably close to laboratory measurements and DNS simulations. Time-, spanwise-, and streamwise-average wall-normal velocity is assumed zero over the transition, with the result that boundary layer thickness triples. Only two parameters need to be assumed: Re_{x_L} and Re_{x_T}. By matching experimental data for local Stanton number, the onset Reynolds number Re_{x_L} is of order 10^5 to 10^6 for smooth plates and decreases as freestream turbulence intensity increases. The completion Reynolds number is bigger than at onset by about a factor of ~2, with the ratio of the final and initial transitional Reynolds numbers $\mathrm{Re}_{x_T}/\mathrm{Re}_{x_L}$ decreasing slightly as Re_{x_L} increases. Overshoot in local wall shear stress and heat flux near the end of the transition region is exhibited by the model, but with a noticeable, unphysical sharpness. The only smoothing in the model is a power-law function used to describe local wall shear stress and heat flux variation in the transition zone. More experimental data are certainly available and could be matched but probably not with much additional demonstration of substance, unless another parametric effect, such as surface roughness, was introduced, which would require data for which surface roughness and freestream turbulence, including axial decay effects, were both well characterized. Such an endeavor seems like a logical next step for both experimental and modeling studies.

Acknowledgment

The author appreciates the support afforded by the H. G. Soo Professorship and NSF grant 2152233 and helpful feedback from Professor Leo Chamorro and anonymous reviewers.

Funding Data

- Division of Atmospheric and Geospace Sciences (Grant No. 2152233; Funder ID: 10.13039/100000159).

Appendix A: Uniform Heat Flux With Unheated Starting Length

The unheated starting length problem with uniform heat flux wall condition has recently been calculated [3] with the following approximate unheated starting length factor, (which has its origins in the uniform wall-temperature case [4]):

$$[1-(x_0/x)^{3/4}]^{-1/3} \tag{A1}$$

This factor (A1), which can also be written as $u_0^{-1/3}$, where $u_0 = 1-(x_0/x)^{3/4}$, is derived from the more exact expression[2] [3]

$$\frac{2.65u_0^{-1/3}}{I(u_0)};\ \text{where}\ I(u_0) = \int_0^1 s^{-2/3}(1-u_0 s)^{1/3}ds \tag{A2}$$

The approximate factor (A1) gives higher predictions than the more exact factor (A2) with the discrepancy being less toward the limit $x_0/x \to 0$ ($u_0 \to 1$), where the unheated length becomes negligible, and more toward the limit, $x_0/x \to 1$ ($u_0 \to 0$), where the unheated length is a large fraction of the total plate length. In the first limit, the exact expression (A2) approaches $2.65/2.65 = 1$, which is matched by Eq. (A1); however, in the second limit, Eq. (A2) approaches $2.65/3 = 0.883$, whereas Eq. (A1) gives 1, representing an error of 12%. The error thus gets systematically larger as x_0/x increases; however, this systematic error can easily be reduced for any x_0/x as follows.

The unheated starting length problem with uniform heat flux wall condition can be solved using the energy integral equation with cubic velocity and temperature profiles. The method is illustrated for uniform wall temperature in Ref. [4] assuming $r = \delta_t/\delta$ is of order one or larger (which is reasonable for gases), where higher-order terms in r with smaller coefficients are neglected. For the uniform heat-flux solution, this means neglecting the term $(3/280)r^3$ compared with $(3/20)r$, which introduces an additional degree of approximation into the solution (beyond the assumed profiles). The resulting unheated starting length factor is simply

$$(1-x_0/x)^{-1/3} \tag{A3}$$

and the numerical coefficient for the St_x expression is 0.418, which by comparison with the case of no unheated starting length, having a coefficient of 0.453, is low by 8%. Adjusting the coefficient accordingly gives Eq. (24). Factor (A3) still systematically over-predicts (A2) but less so than Eq. (A1). The reduction in error associated with Eq. (A3) can be confirmed by evaluating the starting length factors of Eqs. (A1)–(A3). For example, at $x_0/x = 0.1$: $u_0 = 0.822$, $u_0^{-1/3} = 1.07$, $I(u_0) = 2.74$, $2.65u_0^{-1/3}/I(u_0) = 1.03$, and $(1-x_0/x)^{-1/3} = 1.036$, which is within 1% of the more exact value 1.03 (as opposed to 1.07, which is high by 4%); at $x_0/x = 0.5$: $u_0 = 0.405$, $u_0^{-1/3} = 1.35$, $I(u_0) = 2.89$, $2.65u_0^{-1/3}/I(u_0) = 1.24$, and $(1-x_0/x)^{-1/3} = 1.26$, which is within 2% of the more exact value 1.24 (as opposed to 1.35, which is high by 9%); while at $x_0/x = 0.9$: $u_0 = 0.0760$, $u_0^{-1/3} = 2.36$, $I(u_0) = 2.98$, $2.65u_0^{-1/3}/I(u_0) = 2.10$, and $(1-x_0/x)^{-1/3} = 2.15$, which is within 2% of the more exact value 2.10 (as opposed to 2.36, which is high by 12%).

References

[1] Brewster, M. Q., 2014, "Mixed Boundary Layer Skin Friction and Heat Transfer With Abrupt Transition," ASME J. Heat Transfer-Trans. ASME, **136**(11), p. 114501.
[2] Churchill, S. W., 1976, "A Comprehensive Correlating Equation for Forced Convection From Flat Plates," AIChE J., **22**(2), pp. 264–268.
[3] Lienhard, J. H. V, 2020, "Heat Transfer in Flat-Plate Boundary Layers: A Correlation for Laminar, Transitional, and Turbulent Flow," ASME J. Heat Transfer-Trans. ASME, **142**(6), p. 061805.
[4] Kays, W. M., Crawford, M. E., and Weigand, B., 2013, *Convective Heat and Mass Transfer*, 4th ed., McGraw-Hill, New York.
[5] Reynolds, W. C., Kays, W. M., and Kline, S. J., 1958, "Heat Transfer in the Incompressible Turbulent Boundary Layer: I–Constant Wall Temperature," NASA, Washington, DC, Report No. Memorandum 12-1-58W.
[6] Reynolds, W. C., Kays, W. M., and Kline, S. J., 1958, "Heat Transfer in the Incompressible Turbulent Boundary Layer: IV–Effect of Location of Transition and Prediction of Heat Transfer in a Known Transition Region," NASA, Washington, DC, Report No. Memorandum 12-4-58W.
[7] Kestin, J., Maeder, P. F., and Wang, H. E., 1961, "The Influence of Turbulence on the Transfer of Heat From Plates With and Without a Pressure Gradient," Int. J. Heat Mass Transfer, **3**(2), pp. 133–154.
[8] Blair, M. F., 1983, "Influence of Free-Stream Turbulence on Turbulent Boundary Layer Heat Transfer and Mean Profile Development: Part I—Experimental Data," ASME J. Heat Transfer-Trans. ASME, **105**(1), pp. 33–40.
[9] Juliano, T. J., Jewell, J. S., and Kimmel, R. L., 2021, "HIFiRE-5b Boundary-Layer Transition Length and Turbulent Overshoot," J. Spacecr. Rockets, **58**(2), pp. 265–283.
[10] Marxen, O., and Zaki, T. A., 2019, "Turbulence in Intermittent Transitional Boundary Layers and in Turbulence Spots," J. Fluid Mech., **860**, pp. 350–383.
[11] Yao, H., Alves-Portela, F., and Papadakis, G., 2020, "Evolution of Conditionally Averaged Second-Order Structure Functions in a Transitional Boundary Layer," Phys. Rev. Fluids, **5**(9), p. 093902.
[12] Junkhan, G. H., and Serovy, G. K., 1967, "Effects of Free-Stream Turbulence and Pressure Gradient on Flat-Plate Boundary-Layer Velocity Profiles and on Heat Transfer," ASME J. Heat Transfer-Trans. ASME, **89**(2), pp. 169–175.

[2]In Eqs. (B4) and (B6) of Ref. [3] the integrand quantity in square brackets is missing an exponent of –2/3.